Peptide nano-blanket impedes fibroblasts activation and subsequent formation of pre-metastatic niche

Yi Zhou
Zhejiang University
Peng Ke
Shengli Clinical Medical College of Fujian Medical University
Yiyi Xia
Zhejiang University
Honghui Wu
Zhejiang University
Zhentao Zhang
Zhejiang University
Haiqing Zhong
Zhejiang University
Qi Dai
Zhejiang University
Tiantian Wang
Zhejiang University
Mengting Lin
Zhejiang University
Yaosheng Li
Zhejiang University
Xinchi Jiang
Zhejiang University
Qiyao Yang
Zhejiang University
Yiying Lu
Zhejiang University
Xincheng Zhong
Zhejiang University
Min Han
Zhejiang University https://orcid.org/0000-0001-9373-8466
Jianqing Gao (gaojianqing@zju.edu.cn)
Zhejiang University

Article

Keywords: pre-metastatic niche, self-assembled peptide, pre-metastasis associated fibroblasts, 2 vascular endothelial cells, myeloid-derived suppressor cells, tumor metastasis

Posted Date: August 10th, 2021

DOI: https://doi.org/10.21203/rs.3.rs-699014/v1

Version of Record: A version of this preprint was published at Nature Communications on May 25th, 2022. See the published version at https://doi.org/10.1038/s41467-022-30634-8.

Peptide nano-blanket impedes fibroblasts activation and subsequent formation of pre-metastatic niche

Yi Zhou[1], Peng Ke[1 4], Yiyi Xia[1], Honghui Wu[1], Zhentao Zhang[1], Haiqing Zhong[1], Qi Dai[1 5], Tiantian Wang[1], Mengting Lin[1], Yaosheng Li[1], Xinchi Jiang[1], Qiyao Yang[1 5], Yiying Lu[1], Xincheng Zhong[1], Min Han[1 2 3*], Jianqing Gao[1 2 3*]

[1] Institute of Pharmaceutics, Zhejiang Province Key Laboratory of Anti-Cancer Drug Research, College of Pharmaceutical Sciences, Zhejiang University, Hangzhou 310058, P.R. China

[2] Cancer Center of Zhejiang University, Zhejiang University, Hangzhou 310058, P.R. China.

[3] Hangzhou Institute of Innovative Medicine, Zhejiang University, Hangzhou 310058, P.R. China.

[4] Shengli Clinical Medical College of Fujian Medical University, Fuzhou, 350001, China.

[5] Department of Radiation Oncology, Key Laboratory of Cancer Prevention and Intervention, The Second Affiliated Hospital, College of Medicine, Zhejiang University, Hangzhou 310058, China.

* Corresponding author: hanmin@zju.edu.cn (M. H.); gaojianqing@zju.edu.cn (J. G.)

Keywords: pre-metastatic niche, self-assembled peptide, pre-metastasis associated fibroblasts, vascular endothelial cells, myeloid-derived suppressor cells, tumor metastasis

Abstract

In various types of malignant tumors, metastasis is responsible for most of the tumor-induced death. Though emerging technologies provided early detection of tumor metastasis or even warning of high metastatic risk before the actual occurrence of metastasis, clinical treatment on metastasis prevention lags far behind. Evidences have illustrated that primary tumor induced pre-metastatic niche (PMN) formation in distal organs by producing pro-metastasis factors, spreading the spark to ignite the distal microenvironment. Given the fundamental role of PMN in the development of metastases, interruption of PMN formation would be a promising strategy to take early actions against tumor metastasis. Here we report an enzyme-activatable assembled peptide FR17 that can serve as a "flame-retarding blanket" at PMN site specifically to extinguish the "fire" of tumor-supportive microenvironment adaption. Our experiment demonstrated that the assembled peptide successfully reversed extracellular matrix deposition, vascular leakage and angiogenesis through inhibition on fibroblasts activation in PMN, which suppressed the remodeling of metastasis-supportive host stromal, and further prevented the recruitment of myeloid cells to PMN and then recovered the immunosuppressive microenvironment. Cell transcriptomic analysis of the pulmonary recruited MDSC suggested that FR17 intervention could regulate immune response activation, immune cells chemotaxis and migration pathways. Consequently, FR17 administration effectively inhibited pulmonary PMN formation and postoperative metastasis of melanoma, with only 30% lung-metastasis occurrence was observed for FR17 treated group at the time point when 100% occurrence was observed for the control

group and 80% occurrence for anti-PD1 treated group, offering a robust therapeutic strategy against PMN establishing to prevent metastasis.

Introduction

Though therapeutic outcomes and survival rate for patients with various cancers have been greatly improved in last decades, effective treatments for patients with metastatic cancer are still limited[1]. Though emerging technologies provided early detection of malignant transformation or even warning of high metastatic risk by biomarker screening before the actual occurrence of metastasis in clinic[2-6], clinical treatment on metastasis prevention lags far behind. The contemporary therapeutic strategies against metastasis in clinic, including systemic chemotherapy, radiotherapy and immunotherapy, mainly focus on the later time period of metastasis development, or at least after the arrival and colonization of disseminated tumor cells to the distal organs, which have gained unsatisfied clinical outcomes[7-8]. Observations of the adjuvant chemotherapy resistance[6] and treatment-related toxicities[9] revealed the shortcoming of the currently available strategies[10].

Growing evidence illustrated that an inflammatory, neovascularized, immunosuppressive, tumor supportive microenvironment has emerged before the arrival and colonization of disseminated tumor cells, which is termed as pre-metastatic niche (PMN) formation[11]. Relevant studies revealed that complex interactions between multiple participators and alteration in regulative pathways energized the construction of PMN, such as primary tumor-derived cytokines and exosomes, myeloid-derived suppressor cells (MDSCs), and the tumor re-educated stromal environment including pre-metastasis associated fibroblasts, destabilized vasculature and extracellular matrix (ECM) [12, 13] (Fig. 1a).

Since PMN was considered as the foundation laid for circulating tumor cells colonization and one of the vital premises to develop metastasis in distant organs, we wonder if the early process of tumor metastasis can be terminated or even totally prevented by interrupting the formation of PMN. To view the entire process of PMN establishment and metastasis development as a progress of the occurrence and spread of a huge forest fire, it would be more efficient to contain and beat out the local flame by preventing the formation of PMN. Here we report an enzyme-activatable assembled peptide FR17 that can serve as a "flame-retarding blanket" at PMN site specifically, containing and suppressing the "fire blaze" of PMN formation to further develop into overt metastasis (Fig. 1b). As a substrate peptide of matrix metalloproteinase 2 (MMP2), FR17 can release self-assembly monomer FG8 to construct peptide nano-blanket in PMN stromal microenvironment, impeding fibroblasts activation so as to prevent metastatic cascades. We further explored the subsequent impact of inhibition on fibroblasts activation induced by FR17 intervene, revealing the underlining mechanism on cellular interactions among fibroblasts, vascular endothelial cells and extracellular components, and intervention on PMN recruited MDSCs *via in vitro* and *in vivo* experiments.

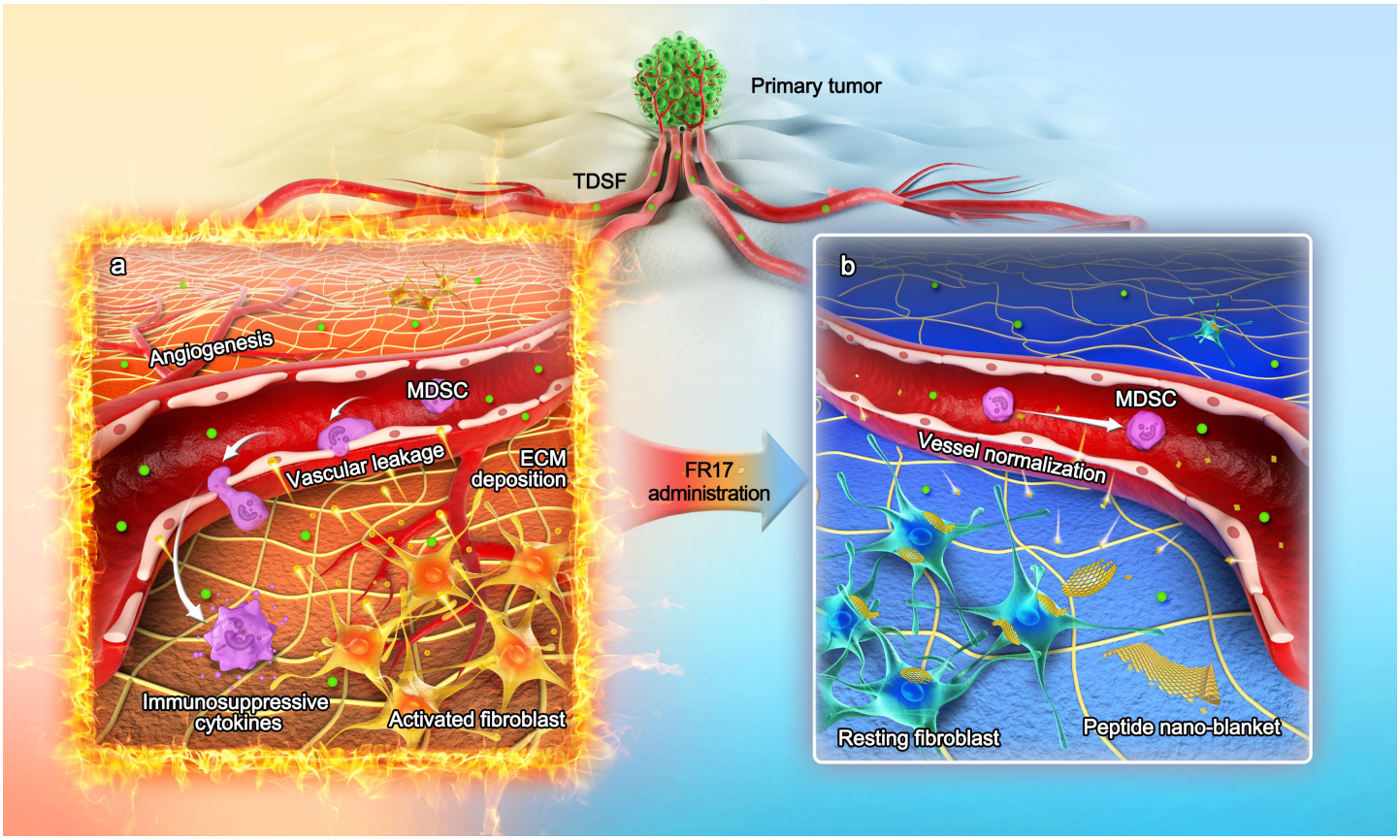

Figure 1. Schematic illustration of peptide nano-blanket impedes fibroblasts activation and subsequent formation of pre-metastatic niche. a, Illustration of the pathological process of pre-metastatic niche (PMN) formation. The primary tumor produces pro-metastasis factors, such as tumor--derived secreted factors (TDSF), to induce fibroblast activation in metastatic destination organs. The tumor-educated activated fibroblasts serve to construct a metastasis-supportive host stromal, including extra cellular matrix (ECM) deposition and reconstruction, angiogenesis and vascular leakage, as well as myeloid-derived suppressor cells (MDSC) recruitment. **b**, After FR17 subcutaneous administration, the *in-situ* assembled peptide nano-blanket in PMN stromal microenvironment impedes fibroblasts activation so as to retard stromal and vessel pro-metastatic reconstruction, inhibiting MDSC recruitment and metastatic cascades.

Results and Discussion

Peptide nano-blanket transformed from FR17.

The matrix metalloproteinase 2 (MMP2)-activatable self-assembled branched peptide (FR17, FFK(GPLGLAGG-YVDKR)Y) consists of (1) the backbone of a self-assembly peptide domain Phe-Phe-Lys-Tyr (FFKY), which is derived from β-amyloid (Aβ) peptide[14, 15]; (2) thymopentin (TP5, Arg-Lys-Asp-Val-Tyr, RKDVY), the pentapeptide with perfect hydrophilic property and immune modulation effect, which is applied as the adjunctive therapeutic agent on cancer treatment in clinic to prevent postoperative infection and to activate immune response[16, 17]. TP5 was conjugated to the side-chain of Lys (K) of the main chain FFKY with the MMP2-cleavable peptide linker (Gly-Pro-Leu-Gly-Leu-Ala-Gly-Gly, GPLGLAGG)[18], increasing the hydrophilic property of the entire peptide molecule. Furthermore, the sequence of TP5 in peptide FR17 was replaced by the scrambled pentapeptide of TP5 without immunomodulatory bioactivity, *i.e.* DVYKR, to form the scrambled group (sFD17, FFK(GPLGLAGG-RKYVD)Y) as peptide assembly control.

Peptides were synthesized *via* Fmoc solid-phase peptide synthesis technology and the peptide sequences were verified by mass spectra (Supplementary Fig. 1-2). When specifically cleaved by MMP2, both FR17 and sFD17 are able to release self-assembled monomer FG8 (FFK(GPLG)Y), constructing peptide self-assemblies, the peptide nano-blanket. The transmission electron microscopy (TEM) images (Fig. 2a) and the Cryo-TEM image (Supplementary Fig. 3a) showed the lamellar structure of the peptide self-assemblies formed by enzymatic degradation (Supplementary Fig. 3b) with an average diameter of ~500 nm (Fig. 2b). In addition, circular

dichroism (CD) analysis revealed alterations in the secondary structure of peptide by the presence of enzyme (Supplementary Fig. 3c). The peptide nano-blanket is woven by the self-assembled monomer FG8 (FFK(GPLG)Y), which would spontaneously fold into lamellar structure rather than the fiber clusters aggregated by FFKY as we previously reported[14]. The peptide assembly relies on the non-bonded interactions, typically hydrogen bonds and π-π stacking, between adjacent peptide molecules. The self-assembling pattern of FG8 changed due to the branch modification with GPLG side-chain. The all-atom molecular dynamics (MD) simulation of FFKY-assemblies and FG8-assemblies gives a microscopic account of the impacts of branch modification on peptide interactions. The MD simulation revealed that there are more intermolecular hydrogen bonds involved in FG8 cluster, which are more ordered and mostly formed between Phe of adjacent FG8 molecules (Supplementary Fig. 4a-b). While the intermolecular hydrogen bonds involved in FFKY assembly are less-formed and disordered (Fig. 2c-h). Besides, the aggregation-induced luminescence effect (AIE) was also employed to monitor the spontaneous aggregation of FG8, the self-assembled monomer, in aqueous system (Supplementary Fig. 4c-e). Taken together, these results indicated the self-assembly property of FG8 monomer, and MMP2-cleaved release of FG8 from FR17 or sFD17 to form the peptide nano-blanket.

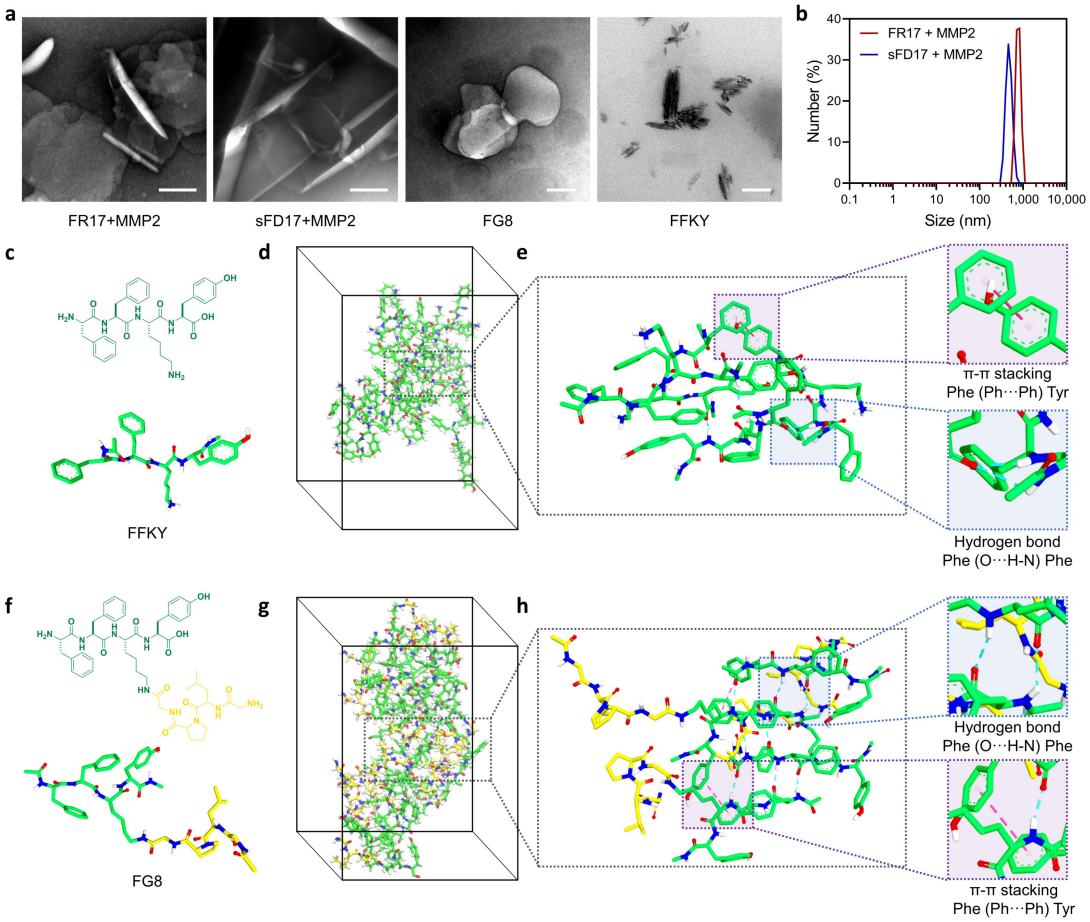

Figure 2. Enzyme-activated self-assembly of FR17 and all-atom molecular dynamics (MD) simulation of the self-assembly of FG8. a, TEM images of FR17 or sFD17 treated with MMP2 (scale bar = 200 nm), FG8 and FFKY (scale bar = 100 nm). **b**, Size distribution of FR17 and sFD17 after MMP2 cleavage. **c**, Molecular structure of FFKY. **d**, The FFKY assemblies generated at t = 200 ns of MD simulation of 16 FFKY molecules in water (containing NaCl for charge neutralization). **e**, Typical molecular cluster and the non-bonded interactions involved in FFKY assemblies in detail. **f**, Molecular structure of FG8. **g**, The FG8 assemblies generated at t = 200 ns of MD simulation of 16 FG8 molecules in water. **h**, Typical molecular cluster and the non-bonded interactions involved in FG8 assemblies in detail. The dashed purple lines denote the π-π stacking. The dashed blue lines denote the hydrogen bonds. The nitrogen atoms are labeled in blue. And the oxygen atoms are labeled in red.

The pathological process in the MCM-induced PMN model *in vivo*

In order to study the effect of FR17 administration on the process of PMN development, an *in vivo* PMN model induced by melanoma-conditioned media (MCM) has been established according to the previous research on PMN[19]. Briefly, tumor-derived factors secreted from primary tumor were replaced by MCM intraperitoneal injection to the mice for 10 consecutive days from Day 1 to 10. On Day 7, when the tumor supportive microenvironment was successfully established in the lung, B16F10 melanoma cells were intravenously administrated as the simulation of circulative tumor cells (CTC) wandering through blood vessels and some would successfully colonize in the prepared "fire scene" in lung (Supplementary Fig. 5b).

The pathological process in the lung was assessed from various aspects during MCM-induced PMN establishment from Day 3 to Day 13 (Supplementary Fig. 5-6). Important cellular derived molecular components and cytokines were closely monitored during the process. The higher expression of the extracellular matrix (ECM) component fibronectin (FN) was generated by MCM inducement. Moreover, matrix metalloproteinase 9 (MMP9), vascular endothelial growth factor a (VEGFa) were up-regulated along with the pathological progress of lung PMN from Day 0 to Day 10 and reached a plateau on Day 10 (Supplementary Fig. 5a). An accordant trend was found on MMP2 level as well (Supplementary Fig. 5d). Meanwhile, the immune cell population analysis during the pathological process in the lung of MCM-induced PMN model was conducted by flow cytometry, which drew our attention to the crime culprit-cell induced PMN, MDSC, for the recruitment of MDSC increased through the timeline (Supplementary Fig. 6-7). It's reported that MDSC contributes a lot in developing the immunosuppression microenvironment in PMN, preparing more suitable and fertile land for tumor cells to take root in[13, 20]. Expression level of the

major inflammatory mediator TGF-β1, possibly produced by MDSCs, increased gradually but sharply. Typical biomarkers produced by MDSC to exert immuno-suppressive effect, in other words, the incriminating tools for the microenvironment re-education, were also detected, *i.e.* reactive oxygen species (ROS), iNOS and arginase-1 (Arg-1) (Supplementary Fig. 5a, c) [21]. Major characteristics of PMN also emerged in lung as time went by, such as activation of fibroblasts (Supplementary Fig. 5e-f), angiogenesis (Supplementary Fig. 5g) and increase of vascular permeability (Supplementary Fig. 5h) [12]. All these data indicated that the *in vivo* PMN model had been well-established, reflecting the pathological process of PMN development. With the overall support provided by PMN, it would consequently accelerate and aggravate metastasis *in vivo* (Supplementary Fig. 8).

FR17 administration interrupts the activation of fibroblast induced by tumor derived factors

According to previous researches on tumor metastasis[22] and our assessment on MCM-induced PMN mice model, the activation of the resident fibroblasts in distal tissues could be regarded as the tipping point of the beginning of PMN establishing, raising the alarm about laying the foundations of the potential metastasis. It's reported that tumor-educated fibroblasts would serve to construct a tumor supportive host stromal *via* TGF-β signaling[23], promoting ECM degradation and reconstruction, inducing angiogenic and pro-inflammatory response of endothelial cells, recruiting VLA-4^+ bone marrow-derived cells (BMDCs) by localized FN deposition for niche formation[19]. Indeed, lysyl oxidase (LOX) cross-linked collagen surrounding pre-metastasis associated fibroblasts attracts $CD11b^+$ myeloid cells invasion in destination organs, which corresponds to metastatic efficiency[24].

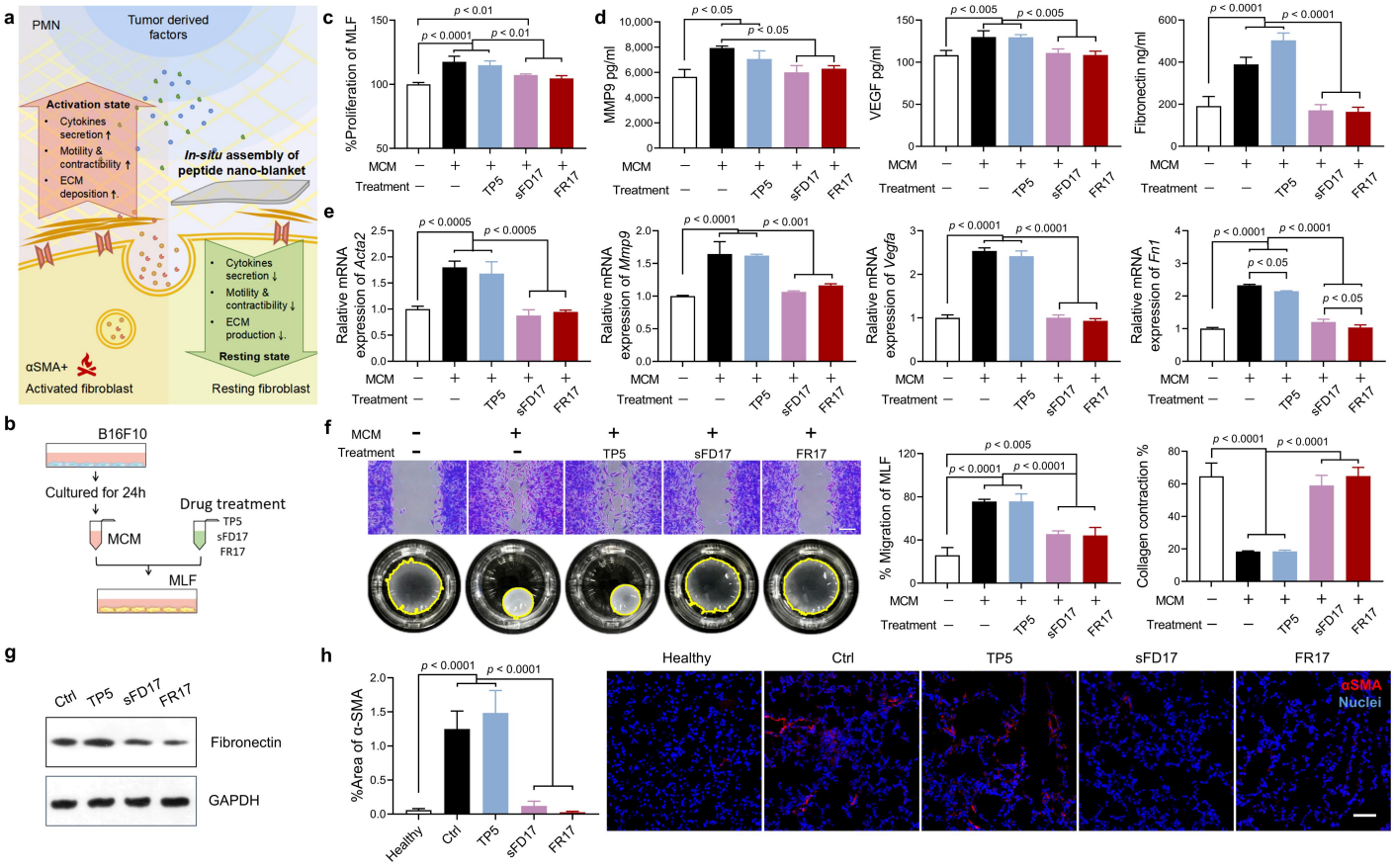

Figure 3. FR17 interrupted the activation of fibroblast induced by tumor derived factors. a, Schematic drawing illustrates the *in-situ* assembled peptide nano-blanket interrupts the activation of fibroblast. When activated by tumor derived factors during PMN development, the expression of proangiogenic factors and ECM remodeling factors would be up-regulated in fibroblast, as well as the ECM components production. While the peptide nano-blanket could calm down fibroblast activation, down-regulating the above factors. **b**, Schematic illustration to show the protocol of MCM stimulation and peptide treatment on mice lung fibroblast (MLF) *in vitro*. **c**, Cell proliferation of MLF after MCM stimulation and peptide treatment (n = 4). **d**, Secretion of MMP9, VEGF and fibronectin in the culture media of MLF after stimulated by MCM, treated with or without peptide. n = 4 for treated groups and 3 for the control group. **e**, qPCR analysis of *Acta2* (*i.e.*, *αSma*), *Mmp9*, *Vegfa*, *Fibronectin1* (*Fn1*) expression in MLF after MCM stimulation

and peptide treatment. **f**, Migration assay and collagen gel contract assay to evaluate MLF cellular functions after MCM stimulation and peptide treatment (n = 3). Scale bar = 100 μm. **g**, Expression level of fibronectin in the lung harvested from the PMN model mice administrated with different peptides on Day 10. **h**, Representative images and semi-quantification of αSMA+ fibroblasts in the lung harvested from mice administrated with different peptides on Day 10. Data is presented as mean ± SD. One-way ANOVA followed by Tukey's multiple comparisons test was employed for statistical evaluation. Scale bar = 50 μm.

Here in a cell model simulating the impact of secreted factors derived from primary tumor on lung fibroblasts *in vitro* (Fig. 3b), FR17 cultivation along with MCM stimulation showed an interruption effect on tumor derived factors irritating lung fibroblasts (Fig. 3a). The treatment with FR17 or sFD17, which would form peptide nano-blanket assembled with the monomer FG8 that was released by MMP2-induced cleavage, successfully prevented the activation of fibroblasts by MCM. The inhibition on the expression of pathologic fibroblast biomarker alpha smooth muscle actin (αSMA) as well as the fibroblasts proliferation and cellular bio-functions (Fig. 3c-f) also substantiated the blocking of lung fibroblasts activity by FR17 or the scrambled control sFD17. The reverse of the increase in cytokines secretion, like MMP9, VEGF, FN, was determined by ELISA kit (Fig. 3d). The qPCR results further suggested that the peptide assemblies might exert biological regulatory effect on cells while not just acting like a physical shield to wrap on the surface of cells (Fig. 3e). Besides, when irritated by tumor derived factors to present the activated αSMA^{+} phenotype, the migration ability as well as the collagen gel

contracting function of fibroblasts got promoted. By contrast, cultivation with FR17 minified these functional changes to a large extent (Fig. 3f). Administration of FR17 to the *in vivo* PMN model also gave great relief to the activation of the fibroblasts in lung (Fig. 3h). What's more, the above data also suggested that the "flame-retarding" effect on fibroblast activation was almost completely contributed by peptide nano-blanket on account of the similar outcomes of the scrambled control sFD17 to that of FR17 treatment.

The stromal microenvironment, apart from fibroblasts, consisting of ECM and vasculature, could also be re-educated by tumor derived factors[25]. For ECM would have gone through remodeling to rebuild a supportive niche for tumor colonization in PMN model, Western blot analysis, Masson staining and Sirius Red staining revealed the down-regulation in the expression of FN (Fig. 3g) and collagen (Supplementary Fig. 9a-c) in the lungs of FR17 group and sFD17 group, which would have likely been over-expressed by the activated fibroblasts otherwise. Besides, versican expression in the lung was also lower in the FR17 or sFD17 intervened groups than that of PMN control group and TP5 treated group (Supplementary Fig. 9d), and the elevated expression of which has been reported to contribute to angiogenesis in tumor[26].

FR17 protects fibroblasts from activation to inhibit vascular leakage and angiogenesis.

The activated fibroblasts in primary tumor, also known as cancer-associated fibroblasts (CAFs), have been reported to produce proangiogenic factors, such as VEGF, so as to promote tumor angiogenesis[27]. What's more, the secretion of MMPs by CAFs induced tumor vascular leakage, exacerbating MDSCs and tumor cells intravasation into the vascular system. Therefore, we

assumed that, as an important participator and vanguard in the construction of PMN, the activated fibroblast may also contribute to angiogenesis and the increasing vascular permeability in PMN (Fig. 4a). Further exploration was carried out on mice vascular endothelial cells to find out whether fibroblasts promote angiogenesis and vascular permeability during the arousement induced by MCM (as shown in Supplementary Fig. 10a). The tube forming assay demonstrated the proangiogenic capability of fibroblasts activated by MCM (Fig. 4b). Meanwhile, the transwell permeability assay (as illustrated in Supplementary Fig. 10b) to mimic the inner layer of blood vessel *in vitro* verified that the fibroblast-conditioned medium (FCM) collected from activated mice lung fibroblasts (MLF) increased vascular permeability (Fig. 4c), indicated directly by the dismission of endothelial adherence junctions mediated by vascular endothelial cadherin, VE-cadherin (Fig. 4d).

For all experiments conducted on endothelial cells, the different conditional FCM was obtained from fibroblasts pre-treated with FR17, sFD17 or TP5 on interrupting MCM stimulation separately. The conditional FCM pre-treated with FR17 or sFD17, rather than TP5, offset the increase in bEnd3 cell proliferation induced by the indirect stimulation of MCM (Supplementary Fig. 10c). The acceleration in neovascularization and the disruption on endothelial cell-cell connection to cause vascular leakage were made up by indirect FR17 or sFD17 treatment on MLF as indicated in Fig. 4b-c.

To examine the influence of FR17 intervention on the expression level of the proangiogenic factors and vascular remodeling enzymes in pulmonary PMN in general, Western blot analysis was carried out. When compared to PMN control group, the increased expression of VEGFa,

ANG2, MMP9, MMP2 was reversed by FR17 treatment almost back to normal levels (Fig. 4e, S11). In addition, the scrambled control sFD17, which doesn't possess the drug-bioactivity of TP5, exhibited similar inhibition result as FR17 while TP5 didn’t, suggesting the protective effect was contributed by the peptide assemblies formed by the enzyme-activatable self-assemble monomer. Vascular leakage assay on PMN model *in vivo* verified that FR17 or sFD17 administration attenuated the enhancement of pulmonary vascular permeability (Fig. 4f-g).

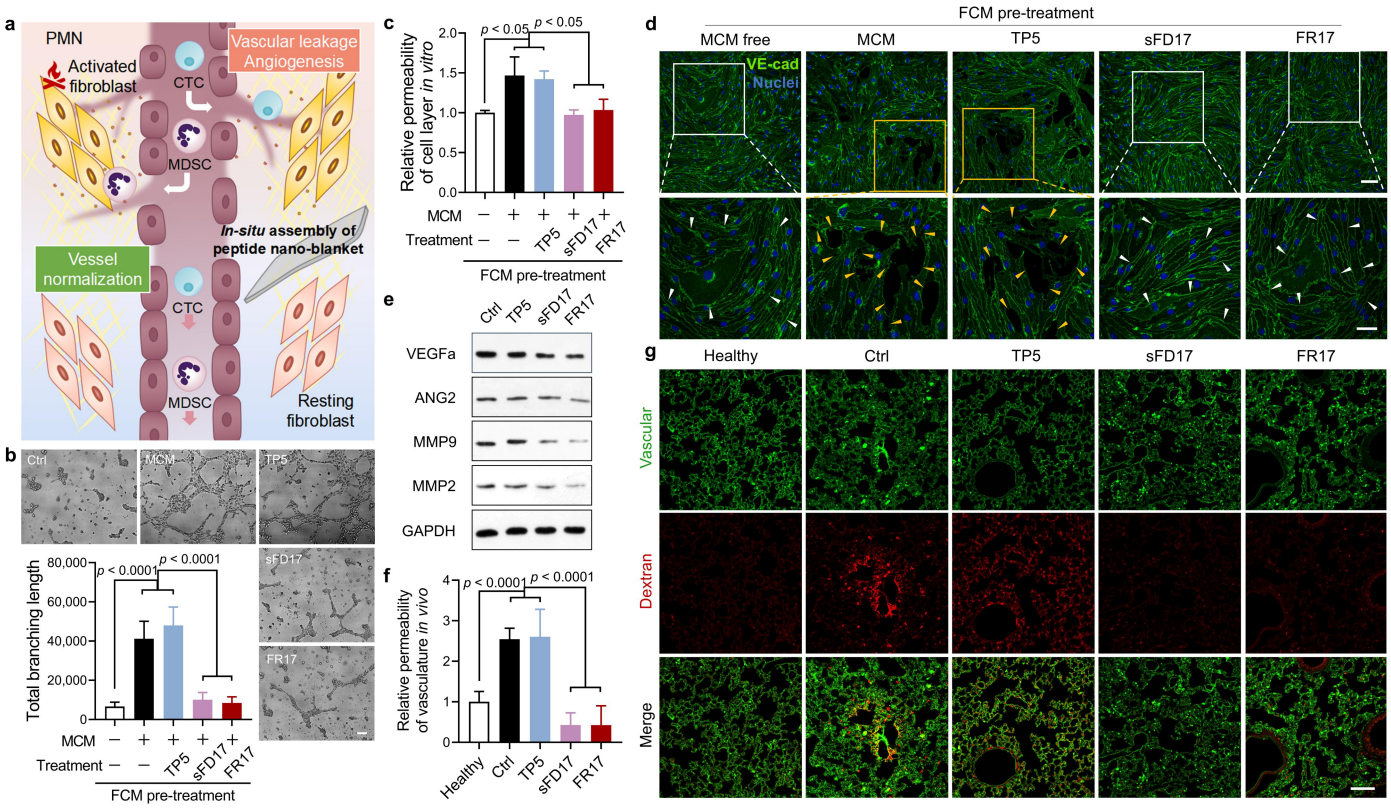

Figure 4. FR17 administration protected fibroblasts from activation to inhibit vascular leakage and angiogenesis. a, Illustration of the inhibition of vascular leakage and angiogenesis *via* the peptide nano-blanket protection on fibroblasts from tumor re-education. **b**, Tube forming assay was performed on bEnd3 cells which were treated with conditional FCM collected from MLF pre-stimulated with MCM and peptide. Scale bar = 100 μm. **c,** Permeability of the endothelial cell layer *in vitro* when co-cultured with MLF pre-treated with MCM and peptide. Data is presented as mean ± SD. n = 3. **d,** Integrality of the endothelial cell monolayer after cultivated with conditional FCM collected from MCM and peptide pre-stimulated MLF, indicated by VE-cadherin on the membrane (n = 3). The white box and the white arrows in the enlarged images indicate the tight junction between the endothelial cells. While the yellow box and yellow arrows indicate the disruption of cell-cell connection. Scale bar = 50 μm in the upper panel. Scale bar = 30 μm in the lower panel. **e**, Expression level of VEGFa, ANG2, MMP9 and

MMP2 in the pulmonary PMN harvested from mice administrated with different peptides on Day 10. **f** & **g**, Vascular permeability of the pulmonary PMN after peptide administration. The semi-quantification was calculated from 5 random visual fields for each section taken from n = 3 biologically independent mice. Data is presented as mean ± SD. Scale bar = 100 μm. One-way ANOVA followed by Tukey's multiple comparisons test was employed for statistical evaluation.

Above data confirmed that FR17 can be employed as an *in-situ* spontaneously-assembled "flame-retarding blanket" to beat out the "flames" on fibroblasts caused by tumor derived factors in PMN, preventing pro-metastatic angiogenesis and vascular destabilization.

FR17 administration impedes MDSC recruitment to pulmonary PMN and modulates the immuno-microenvironment.

Given the fact that MDSC occupies a vital position in PMN construction and metastasis formation, MDSC has attracted wide concerns in recent years. It's firstly reported by David Lyden's team that $VEGFR^+$ myeloid progenitor cells are recruited and formed cell clusters to the sites highly expressing FN, which is most likely produced by resident fibroblasts, in the distal tissues prior to the arrival of tumor cells[19]. The recruitment of MDSC was found to be related to the enhancement of ECM production and remodeling in PMN, including cross-linking collagen by LOX secreted by tumor cells[24], FN deposition[28], periostin (POSTN)-enrichment[29]. As MDSC plays a crucial role in developing immunosuppressive and inflammatory microenvironment,

some pioneers have demonstrated that blocking the recruitment of MDSC could be a promising strategy to suppress early metastasis by preventing the development of breeding ground for tumor[30-33].

In our PMN model, the accumulation of MDSC in lung was decreased in FR17 and sFD17 groups, revealed by immunofluorescent staining (Fig. 5a) and flow cytometry analysis on Day 10 (Fig. 5b). Moreover, focal enrichment areas of FN and the co-localization of LOX attracted an increasing number of $CD11b^{+}Gr^{+}$ MDSC in serial sections of the PMN lung comparing to healthy lung (Fig. 5a, Supplementary Fig. 12), consistent with the previous reports[24]. The immunofluorescent stains indicated that FR17 intervention successfully down-regulated the expression of LOX, FN and POSTN in the lung induced by tumor-derived factors to impede the construction of PMN, which probably resulted in the cut in MDSC recruitment (Supplementary Fig. 12). To evaluate prevention of peptide administration on developing PMN immunosuppressive environment, protein level of TGF-β in PMN (Fig. 5c), the well-known immuno-modulator produced by MDSC to regulate the establishment of immunosuppressive tumor supportive niche, as well as the pro-inflammatory cytokine IL-6 was detected (Fig. 5d). FR17 treatment successfully down-regulated TGF-β and IL-6 expression in lung, so as sFD17. In the meantime, TP5 administration exhibited partial abatement on the expression of these cytokines[34], suggesting both the enzyme-responsive assembled peptide nano-blanket and the immunoregulatory agent TP5 facilitated the normalization of immunosuppressive and inflammatory environment of PMN.

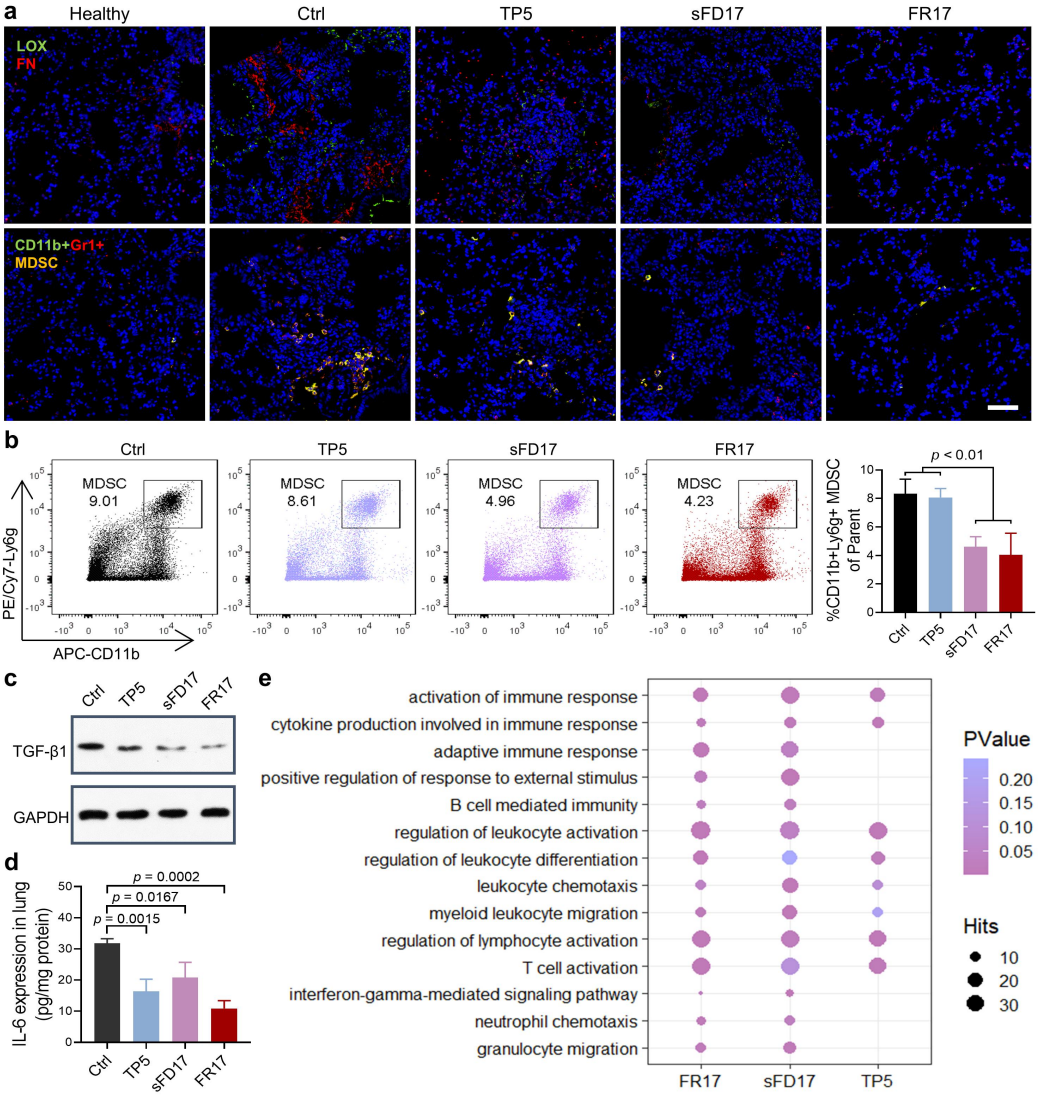

Figure 5. FR17 administration prevented MDSC recruitment, pausing the development of the immunosuppressive microenvironment in PMN. a, Serial sections of the lungs harvested from the model mice treated with different peptides. Serial sections show the distribution of lysyl oxidase (LOX) and Fibronectin (FN) and the co-location of $CD11b^{+}Gr1^{+}$ myeloid derived suppressor cells (MDSC). **b**, Recruitment of $CD11b^{+}Ly6g^{+}$ MDSC to the lungs of the model mice treated with different peptides on Day 10. Data is presented as mean ± SD. n = 4 biologically independent mice for treatment groups, n = 3 for the control group. **c**, Expression of TGF-β1 in the lung harvested from PMN model mice administrated with different peptides. **d**,

IL-6 expression in the lung tissue fluid collected from PMN model mice administrated with different peptides. Data is presented as mean ± SD. n = 3 biologically independent mice. One-way ANOVA followed by Tukey's multiple comparisons test was employed for statistical evaluation. **e**, GO enrichment analysis of $CD11b^{+}Ly6g^{+}$ MDSC sorted from different treatment groups. RNA preparations were extracted from $CD11b^{+}Ly6g^{+}$ MDSCs sorted from lungs pooled from 10-12 mice per sample. The size of the dots corresponds to the number of genes per pathway, and the color indicates *p*-value. Statistical significance was considered at least at $p < 0.05$.

To find out whether the impact on MDSC-induced immunosuppressive microenvironment in PMN was mainly contributed by TP5 or by the *in-situ* assembled peptide nano-blanket, cell transcriptomic analysis of MDSCs recruited to the lung was carried out on different treatment groups. Given the fact that $CD11b^{+}Ly6g^{+}$ MDSC takes the majority (over 90%) of MDSC population in the lung of MCM-induced PMN model (Supplementary Fig. 6a-b), $CD11b^{+}Ly6g^{+}$ MDSC were sorted on Day 10 from pulmonary PMN after different treatments as the representative subset for further transcription analysis (Supplementary Fig. 13). GO enrichment analysis indicated that the regulation effect of FR17 might relate to the activation of immune response pathway, cytokine production involved in immune response, regulation of leukocyte and lymphocyte activation, leukocyte chemotaxis and migration (Fig. 5e). Relative enriched pathways provided possible comments on the underlined mechanisms, including: regulation on cytokine biosynthetic process, adaptive immune response based on somatic recombination

immune receptors built from immunoglobulin super-family domains, interferon-γ-mediated signaling pathway and the impact on chemokine receptor binding as well as CXCR chemokine receptor binding (Supplementary Fig. 14). From above, when compared with the differential gene enrichment pathway of sFD17 and TP5, we found that the regulation on immune cells chemotaxis and migration pathways was contributed by the *in-situ* peptide assemblies, for the peptide nano-blanket would only form in FR17 or sFD17 treated lung while not in free TP5 treated group. And the Venn diagram and further enrichment analysis to put TP5 aside suggested these would correspond to the regulation on cell surface receptor signaling pathway by peptide assemblies (Supplementary Fig. 14b-c). In addition, the regulation on leukocyte differentiation and T cell activation pathway was mainly contributed by TP5 (Supplementary Fig. 14d), which has been commonly accepted as one of the mechanisms for TP5 to exert immune regulation effect[35-37].

Moreover, the *in-situ* assembled peptide nano-blanket formed by FR17 inhibited tumor cells migration as well, with hardly any effect on cell viability (Supplementary Fig. 15).

FR17 administration inhibits melanoma lung metastasis *in vivo*.

First, we evaluated the anti-metastasis efficacy of FR17 on MCM-induced lung metastasis model. C57/BL6 mice were pre-induced by MCM administration for 10 days to set up the tumor supportive pre-metastatic niche in lung. Tumor cells were then injected through the tail vein on Day 7 to simulate the circulative tumor cells (CTC) wandering through blood vessels and eventually settled down in pulmonary PMN. As illustrated in Fig. 6a, peptide subcutaneous

administration started from Day 3 and ended at 2 weeks-post lung tumor inoculation. The metastasis inhibition efficacy was evaluated in terms of the tumor module number on Day 28. FR17 effectively suppressed tumorigenesis and the development of metastasis in lung, compared to both the control and TP5 groups (Fig. 6b-d). Moreover, the good outcomes of sFD17 treatment which was close to that of FR17 group emphasized the main role of nano-blanket assembled by the enzyme-activated released monomer in intervening PMN construction. Therefore, the *in-situ* assembled nano-blanket also played a part in inhibiting metastasis development and growth. Preliminary safety evaluation on these model mice at the end of the experiment revealed no severe safety concern of FR17 administration (Supplementary Fig. 16-17). The systemic immune modulation effect of TP5 was reflected on the recovery of thymus shrinking as well (Supplementary Fig. 16d, 17). What's more, peptide administration prevented tumor cells infiltration into the spleen (Supplementary Fig. 17).

The anti-metastasis activity of FR17 was further verified on a post-surgery metastasis model[30] (illustrated by Fig. 6e), which is closer to the clinical treatment of resectable melanoma followed-up with adjuvant therapy for patients at high risk of recurrence. Here we compared FR17 therapy with the rising-star of checkpoint inhibitors, PD1 antibody[38-39], which was approved by FDA as adjuvant therapy on primary tumor excised with lymph node management or metastatic melanoma[40]. As demonstrated in Fig. 6f, the recurrence of lung metastasis was put off and the overall survival was greatly improved by FR17 therapy when compared with control (Fig. 6g-i). The median overall survival prolonged for 23.3% (from 30 days to 37 days), catching up with the outcomes of anti-PD1 treatment (from 30 days to 36 days). And the median

lung-metastasis-free survival prolonged from less than 19 days of both control group and anti-PD1 treated group to 23 days of FR17 treated group. At the first time-point for lung metastasis monitoring *via* bioluminescence imaging, lung metastasis has been observed in all of the 10 mice from the control group, 8 mice from anti-PD1 treated group while only 3 mice from FR17 treated group on Day 19. The retard of the occurrence of lung metastasis after FR17 administration emphasized the importance of PMN intervention. What's more, the relapse rate of the primary tumor post-resection was reduced from 10 / 10 in the control group to 4 / 10 in FR17 treated group (Supplementary Fig. 18).

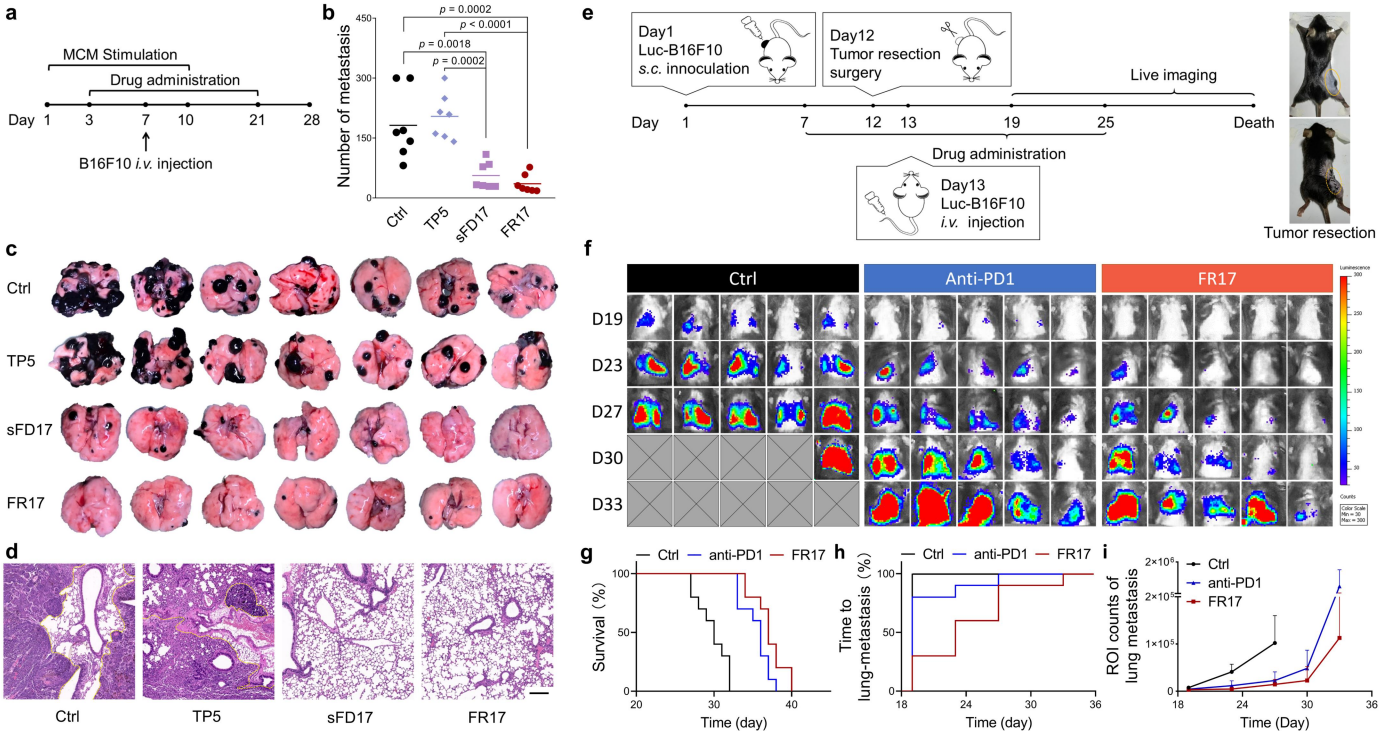

1 **Figure 6. FR17 administration inhibited lung metastasis *in vivo* by retarding PMN**
2 **formation. a**, Schedule of MCM-induced lung metastasis model with peptide treatment. Peptide
3 administration started from Day 3 for metastasis prevention. **b**, Number of the metastatic nodules
4 in the lung of different treatment groups (n = 7). Data is presented as mean ± SD. One-way
5 ANOVA followed by Tukey's multiple comparisons test was employed for statistical evaluation.
6 **c**, Images of the lung metastasis harvested on Day 28 from different treatment groups. **d**,
7 Representative images of Hematoxylin & Eosin staining of lung sections from different
8 treatment groups. The lung metastasis is circled by yellow dotted lines. Scale bar = 200 μm. **e**,
9 Schedule of post-surgery metastasis model. Peptide administration started from Day 7 to 25. **f**,
10 Representative *in vivo* bioluminescent images of mice without treatment or treated with FR17 or
11 anti-PD1 (n = 10). The grey patches represent dead mice in the control group. **g**, Survival curves
12 of the mice treated with FR17 or anti-PD1 or without treatment (n = 10). **h**, The cumulative

incidence of new pulmonary metastases in the mice treated with FR17 or anti-PD1 or without treatment (n = 10). **i**, Semi-quantification of the *in vivo* bioluminescent signals in the lungs of the mice treated with FR17 or anti-PD1 or without treatment (n = 5). Data is presented as mean ± SD.

Conclusions

In summary, we have explored the magical retarding effect of the PMN microenvironment responsive-assembled peptide nano-blanket on fibroblasts activation, impeding PMN development. The enzyme-activatable assembled peptide FR17 can be enzyme-cleaved to release the self-assembly monomer FG8 to construct a lamellar structure, which is named as peptide nano-blanket. Experiments demonstrated that FR17 administration not only beat out the "flame" set up on resident fibroblasts induced by tumor derived factors, but also interrupted the subsequent PMN formation, including preventing pro-metastatic angiogenesis and vascular destabilization, and then intervening MDSCs' recruitment as well as their bio-functions. Astonishingly, when treated with sFD17, tumor-induced fibroblast activation was also impeded by peptide-assemblies without the assistance of TP5 so as to arrest the following pro-metastatic pathological process. This finding illustrated that the "flame-retarding" effect on fibroblast activation could be contributed by the drug-free peptide nano-blanket alone, presenting a broad application prospect of drug-free peptide assemblies to regulate PMN microenvironment and to prevent tumor distant metastasis. This work also elucidated the important role of pre-metastasis associated fibroblast in the complex interactions between major participators in PMN formation

and metastasis development, suggesting that reprogramming or intervention on the key juncture could make a big difference on fighting against tumor metastasis.

References

1. Gdowski, A. S., Ranjan, A. & Vishwanatha, J. K. Current concepts in bone metastasis, contemporary therapeutic strategies and ongoing clinical trials. *J. Exp. Clin. Cancer Res.* **36,** 108-121 (2017).
2. Pashayan, N. & Paul, P. D. P. The challenge of early detection in cancer. *Science (New York, N.Y.)* **368,** 589-590 (2020).
3. Rodriguez-Ruiz, A. et al. Stand-alone artificial intelligence for breast cancer detection in mammography: Comparison with 101 radiologists. *J. Natl. Cancer Inst.* **111,** 916-922 (2019).
4. Poudineh, M., Sargent, E. H., Pantel, K., Kelley, S. O. Profiling circulating tumour cells and other biomarkers of invasive cancers. *Nat. Biomed. Eng.* **2,** 72-84 (2018).
5. Christensen, E. et al. Early detection of metastatic relapse and monitoring of therapeutic efficacy by ultra-deep sequencing of plasma cell-free DNA in patients with urothelial bladder carcinoma. *J. Clin. Oncol.* **37,** 1547-1557 (2019).
6. Abbosh, C. et al. Phylogenetic ctDNA analysis depicts early-stage lung cancer evolution. *Nature* **545,** 446-451 (2017).
7. Curti, B. D. & Faries, M. B. Recent advances in the treatment of melanoma. *N. Engl. J. Med.* **384,** 2229-2240 (2021).

8. Oliver Sartor, M. D. & Johann S. de Bono, M. B. Metastatic prostate cancer. *N. Engl. J. Med.* **378,** 645-657 (2018).

9. Zhang, C. et al. Radiotherapy and cytokine storm: Risk and mechanism. *Front. Onco.* **11,** 670464 (2021).

10. Cardoso, F. et al. 70-Gene signature as an aid to treatment decisions in early-stage breast cancer. *N. Engl. J. Med.* **375,** 717-29 (2016).

11. Peinado, H. et al. Pre-metastatic niches: organ-specific homes for metastases. *Nat. Rev. Cancer* **17,** 302-317 (2017).

12. Liu, Y. & Cao, X. Characteristics and significance of the pre-metastatic niche. *Cancer Cell* **30,** 668-681 (2016).

13. Zhou, Y., Han, M., & Gao, J. Q. Prognosis and targeting of pre-metastatic niche. *J. Control. Release* **325,** 223-234 (2020).

14. Wang, T. T. et al. AIE/FRET-based versatile PEG-Pep-TPE/DOX nanoparticles for cancer therapy and real-time drug release monitoring. *Biomater. Sci.* **8,** 118-124 (2020).

15. Guo, W. W. et al. Intracellular restructured reduced glutathione-responsive peptide nanofibers for synergetic tumor chemotherapy. *Biomacromolecules* **21,** 444-453 (2020).

16. Zeng, F. L. et al. Clinical efficacy and safety of synthetic thymic peptides with chemotherapy for non-small cell lung cancer in China: A systematic review and meta-analysis of 27 randomized controlled trials following the PRISMA guidelines. *Int. Immunopharmacol.* **75,** 105747 (2019).

17. Li, S. et al. Supramolecular nanofibrils formed by coassembly of clinically approved drugs for tumor photothermal immunotherapy. *Adv. Mater.* **33,** e2100595 (2021).

18. Qin, S. Y. et al. Theranostic GO-based nanohybrid for tumor induced imaging and potential combinational tumor therapy. *Small* **10,** 599-608 (2014).

19. Kaplan, R. N. et al. VEGFR1-positive haematopoietic bone marrow progenitors initiate the pre-metastatic niche. *Nature* **438,** 820-827 (2005).

20. Engblom, C., Pfirschke C. & Pittet M. J. The role of myeloid cells in cancer therapies. *Nat. Rev. Cancer* **16,** 447-462 (2016).

21. Gabrilovich, D. I. Myeloid-derived suppressor cells. *Cancer Immunol. Res.* **5,** 3-8 (2017).

22. Pein, M. et al. Metastasis-initiating cells induce and exploit a fibroblast niche to fuel malignant colonization of the lungs. *Nat. Commun.* **11,** 1494 (2020).

23. Kong, J. et al. Extracellular vesicles of carcinoma-associated fibroblasts creates a pre-metastatic niche in the lung through activating fibroblasts. *Molecular Cancer* **18,** 175 (2019).

24. Erler, J. T. et al. Hypoxia-induced lysyl oxidase is a critical mediator of bone marrow cell recruitment to form the premetastatic niche. *Cancer Cell* **15,** 35-44 (2009).

25. Paolillo, M. & Schinelli, S. Extracellular matrix alterations in metastatic processes. *Int. J. Mol. Sci*. **20,** 4947 (2019).

26. Asano, K. et al. Stromal versican regulates tumor growth by promoting angiogenesis. *Sci. Rep.* **7,** 17225 (2017).

27. Zhou, X. et al. Melanoma cell-secreted exosomal miR-155-5p induce proangiogenic switch of cancer-associated fibroblasts *via* SOCS1/JAK2/STAT3 signaling pathway. *J. Exp. Clin. Cancer Res.* **37,** 242 (2018).

28. Murgai, M. et al. KLF4-dependent perivascular cell plasticity mediates pre-metastatic niche

formation and metastasis. *Nat. Med*. **23,** 1176-1190 (2017).

29. Wang, Z. et al. Periostin promotes immunosuppressive premetastatic niche formation to facilitate breast tumour metastasis. *J. Pathol*. **239,** 484-495 (2016).

30. Long, Y. et al. Self-delivery micellar nanoparticles prevent premetastatic niche formation by interfering with the early recruitment and vascular destruction of granulocytic myeloid-derived suppressor cells. *Nano Lett*. **20,** 2219-2229 (2020).

31. Jiang, T. et al. Metformin and Docosahexaenoic Acid Hybrid Micelles for Premetastatic Niche Modulation and Tumor Metastasis Suppression. *Nano lett.* **19,** 3548-3562 (2019).

32. Lu, Z et al. Epigenetic therapy inhibits metastases by disrupting premetastatic niches. *Nature* **579,** 284-290 (2020).

33. Kaczanowska, S. et al. Genetically engineered myeloid cells rebalance the core immune suppression program in metastasis. *Cell* **184,** 2033-2052 (2021).

34. Lunin, S. M. et al. Thymic peptides restrain the inflammatory response in mice with experimental autoimmune encephalomyelitis. *Immunobiology* **218,** 402-7 (2013).

35. Cascinelli, N. et al. Evaluation of clinical efficacy and tolerability of intravenous high dose thymopentin in advanced melanoma patients. *Melanoma Res.* **8,** 83-9 (1998).

36. Wang, Y. et al. The novel role of thymopentin in induction of maturation of bone marrow dendritic cells (BMDCs). *Int. Immunopharmacol.* **21,** 255-60 (2014).

37. Lunin, S. M. et al. Thymus peptides regulate activity of RAW 264.7 macrophage cells: inhibitory analysis and a role of signal cascades. *Expert Opin. Ther. Targets* **15,** 1337-46 (2011).

38. Rizvi, N. A. et al. Activity and safety of nivolumab, an anti-PD-1 immune checkpoint

inhibitor, for patients with advanced, refractory squamous non-small-cell lung cancer (CheckMate 063): a phase 2, single-arm trial. *Lancet Oncol.* **16,** 257-65 (2015).

39. Gong, N. et al. Proton-driven transformable nanovaccine for cancer immunotherapy. *Nat. Nanotechnol.* **15,** 1053-1064 (2020).

40. NIH. National Cancer Institute, Melanoma Treatment (PDQ#)-Health Professional Version. Available from: https://www.cancer.gov/types/skin/hp/melanoma-treatment-pdq#_402.

Acknowledgements

This work was supported by the National Natural Science Foundation of China (Nos. 81673022). We thank Professor Yu Kang at College of Pharmaceutical Sciences, Zhejiang University for guidance on molecular dynamics simulation. We thank Qichun Wei's lab for providing the luciferase transfected B16F10. We thank Qin Han, Chenyu Yang, and Dandan Song at the Center of Cryo-Electron Microscopy (CCEM), Zhejiang University for their technical assistance on Confocal laser scanning microscopy and transmission electron microscopy. We thank Yanwei Li at the Core Facilities of Zhejiang University School of Medicine for technical assistance in flow cytometry analysis.

Author Contributions

M.H. and Y.Z. conceived the project and designed the experiments. M.H. and J.G. supervised the project, discussed and commented on the manuscript. Y.Z. performed the majority of the experiments and data analysis. P.K. assisted with cell culture of B16F10, preparing MCM and animal experiments. Y.X. synthesized and characterized TPE-FR17 and TPE-FFKY. H.W. assisted with the establishment of animal models. Y.Z. performed the flow cytometry experiments with assistance from Z.Z., T.W., M.L., P.K., Y.S.L., Y.X., H.Z., X.Z. and Q.Y.; Y.Y.L. supported the operation of confocal microscope. Y.Z., Q.D., P.K., H.Z., Y.X., Y.S.L., X.J. and H.W. operated the tumor resection surgery. Y.Z. wrote the manuscript. All authors discussed the results and commented on the manuscript.

Competing Interests statement

All the authors declare no conflicting interests.

Methods

Characterization of FR17 and sFD17. Peptide FR17 and sFD17 were synthesized *via* Fmoc solid-phase peptide synthesis technology by APeptide Shanghai. The molecule structure and amino acid sequence of peptide were confirmed by mass spectra.

Enzyme induced assembly of FR17 and sFD17. Peptide FR17 or sFD17 was dissolved in HBS buffer (pH 7.4, containing 50 mM HEPES, 150 mM NaCl, 10 mM $CaCl_2$) at 500 μM. Activated hMMP2 was added to the peptide solution at the working concentration of 1 μg/mL. The solutions were then incubated in 37 °C air-bath for 24 h. The size of the enzyme treated sample, which has formed the peptide nano-blanket, was measured by Zetasizer Nano ZS (Malvern Instruments). The assembly morphology of the assembled nano-blanket was observed with transmission electron microscope (FEI Tecnai G2 spirit) for TEM image and 200kv transmission electron microscope (FEI Talos F200C) for Cryo-TEM image.

All-atom molecular dynamics simulation. The molecular structures of peptide FFKY and FG8 monomer were first constructed *via* AMBERTOOL based on the AMBER14SB force field. Dynamics simulation runs were performed utilizing Gromacs 2018.4 package[1]. System configurations were visualized using VMD software[2], and generated into images mainly employing GRACE software. The simulation was performed in water boxes containing 16 FFKY or FG8 molecules. FFKY system was simulated containing NaCl to neutralize electric charge of

the amidogen on the side-chain if Lys. Energy was minimized according to the steepest-descent method. Bond lengths were constrained by the LINCS algorithms. The nonbonded LJ interactions were cut off at 1.2 nm. Electrostatics was treated utilizing the Particle Mesh Ewald (PME) scheme. All production runs were simulated in the NPT ensemble using V-rescale coupling scheme with the temperature maintained at 298.15 K and parrinello-rahman coupling scheme with pressure kept at 1.0 bar and isotropic coupling type. The time constants for the pressure and temperature couplings were respectively set to 2.0 and 0.2 ps. Besides, the compressibility value was 4.5×10^{-5} bar^{-1}. Periodic boundary conditions with a time step of 0.002 ps were adopted. Simulations were carried out for 200 ns and the structural coordinate information was recorded per 50 ps.

Cell lines and cell culture. B16F10 cells were purchased from Cell Bank of Chinese Academy of sciences (Shanghai, China) and cultured in Dulbecco's Modified Eagle Medium (DMEM, Cienry, China) containing 10% (v/v) fetal bovine serum (FBS, Gibco, Grand Island, USA) and penicillin-streptomycin Solution (100×, TBD, Tianjin, China) at 1% (v/v). And the luciferase transfected B16F10 (Luc-B16F10) was kindly gifted by Qichun Wei’s lab, the Second Affiliated Hospital, Zhejiang University. The mouse lung fibroblasts (MLF) were purchased from iCell Bioscience Inc. (Shanghai, China) and cultured in Dulbecco's Modified Eagle Medium/Nutrient Mixture F-12, 1:1 mixture (DMEM/F12 medium, Multicell, Wisent Int., Canada) containing 10% (v/v) fetal bovine serum (FBS, Gibco, Grand Island, USA) and penicillin-streptomycin Solution (100×, TBD, Tianjin, China) at 1% (v/v). The mouse endothelial cells bEnd3 was kindly gifted

by Fuqiang Hu's lab, Institution of Pharmaceutics, College of Pharmaceutical Sciences, Zhejiang University. The bEnd3 cells were cultured in the same medium as B16F10. Cells were cultured in a cell incubator containing 5% CO_2 at 37 °C and passaged when reached 80%-90% confluence. The melanoma-conditioned medium (MCM) was obtained as follows: when B16F10 reached 70-80% confluence, washed with PBS and changed the medium to serum-free medium and incubated for 24 h. The cell supernatants were collected, centrifuged at 2000 rpm for 10 min to discard the cell debris. The MLF-conditioned medium (FCM) was obtained as follows: MLFs were stimulated by MCM (supplemented with 10% (v/v) FBS) with or without peptide drugs (TP5, sFD17, FR17 at the concentration of 100 μM) for 48 h, then replaced with fresh complete medium and incubate for another 24 h. The cell supernatants were collected, centrifuged at 2000 rpm for 10 min to discard the cell debris.

Cell proliferation assays. MLFs in rapid proliferation were plated in 96-well plates at the density of 4×10^3 per well and cultured overnight. Former media were removed and the cells were cultivated with 100 μL MCM supplemented with 10% (v/v) FBS, treated with or without peptide drugs (TP5, sFD17, FR17 at the concentration of 100 μM). Cells cultivated with fresh complete medium was set up as control. After incubation for 48 h, cell proliferation was measured using a Cell Counting Kit-8 assay (Cat. 13E02A60, Boster Biotech., China) according to the manufacturer's instructions. The optical density at 450 nm (OD_{450} nm) was measured using a multiwell plate reader (ELX800, BioTek, USA). Each group was repeated at least 4 times, and cell proliferation was presented as mean ± SD.

Cytokines secretion and gene expression of MLFs. An equal number of MLFs in rapid proliferation were seeded in a 24-well plate per well, cultivated with MCM supplemented with 10% (v/v) FBS, treated with or without peptide drugs (TP5, sFD17, FR17 at the concentration of 100 μM) for 48 h in at least triplicate. Cells cultivated with fresh complete medium was set up as control. The cell supernatants were collected, centrifuged at 2000 rpm for 5 min to discard cell debris. MMP9 ELISA kit (EK0466, Boster Biotech., China) and VEGF ELISA kit (EK0541, Boster Biotech., China) were employed to measure the secretion level of MMP9 and VEGF in the cell supernatant. An equal number of MLFs in rapid proliferation were seeded in 24-well plate cultivated with (serum-free) MCM, treated with or without peptide drugs (TP5, sFD17, FR17 at the concentration of 100 μM) for 48 h in quadruplicate. Cells cultivated with fresh DMEM/F12 medium was set up as control. The cell supernatants were collected, centrifuged at 2000 rpm for 5 min to discard cell debris. The secretion of FN was measured by FN ELISA kit (EK0351, Boster Biotech., China) according to the manufacturer's instructions. Cells with different treatments were harvested for RT-qPCR analysis to determine the gene expression level of *M-Acta2* (Mouse αSMA), *M-Mmp9*, *M-Vegfa* and *M-Fn1*. The primer sequences are provided as follows:

M-Gapdh-F: 5' GGTTGTCTCCTGCGACTTCA 3' 58.2

M-Gapdh-R: 5' TGGTCCAGGGTTTCTTACTCC 3' 58.2 183bp

M-Vegfa-F: 5' GCTACTGCCGTCCGATTGAG 3' 60.87

M-Vegfa-R: 5' ACTCCAGGGCTTCATCGTTACAG 3' 62.25 132bp

M-Mmp9-F: 5' CACAGCCAACTATGACCAGGAT 3' 59.1

M-Mmp9-R: 5'	CAGGAAGACGAAGGGGAAGA	3'	59.1	115bp
M-Fn1-F: 5'	CTATTTACCAACCGCAGACTCAC	3'	58.7	
M-Fn1-R: 5'	TGCTTGTTTCCTTGCGACTT	3'	58.5	115bp
M-Acta2-F: 5'	CAACTGGTATTGTGCTGGACTC	3'	57.3	
M-Acta2-R: 5'	ATCTCACGCTCGGCAGTAGT	3'	57.3	181bp

Cell Migration assays. MLFs in rapid proliferation were plated in Culture-Inserts (2 Well, Ibidi, Germany) at the density of 1×10^5 in 70 μL per well and grew to confluence overnight. Culture-Inserts as well as the former medium were gently removed. Then the MLFs were cultivated with MCM supplemented with 10% (v/v) FBS, treated with or without peptide drugs (TP5, sFD17, FR17 at the concentration of 100 μM) in triplicate. Cells cultivated with fresh complete medium was set up as control. Pictures of the cell scratches were taken under the microscope at 0 h. After incubated for 24 h, MLFs were fixed and stained with crystal violet. Pictures were taken and analyzed with ImageJ.

Collagen gel contraction assay. An equal number of MLFs seeded in 6 cm dishes were cultivated with MCM supplemented with 10% (v/v) FBS, treated with or without peptide drugs (TP5, sFD17, FR17 at the concentration of 100 μM) for 48 h. Cells cultivated with fresh complete medium was set up as control. The pre-treated MLFs were digested and re-suspended at the density of 2×10^6 per mL, kept on ice for later use. The neutral collagen solution was prepared as follows: 224 μL type I collagen gel (3 mg/ml, Cat. C8062, Solarbio, China) was

quickly mixed with 100 μL conditional medium and 8 μL NaOH (0.1 N) on ice. Then 300 μL of the pre-treated MLFs suspension was added to the collagen solution on ice immediately. And the neutral cell-collagen mixture was added to 48-well plates 200 μL per well in triplicate and allowed to solidify for 45 min at room temperature. After incubated at 37 °C for 12 h, the gels were photographed. ImageJ software was used to measure gel area and evaluate contraction. Gel contraction was assessed as the ratio of the gel area to the area of the well.

Tube forming assay. Mouse endothelial bEnd3 cells seeded in 6 cm dishes were cultivated with conditional FCM (from MLF previously stimulated by MCM with or without TP5, sFD17 or FR17 peptide as illustrated above) for 24 h. The cells were harvested and seeded in 48-well plates pre-coated with Matrigel (Cat. 356230, BD, USA) in triplicate for each group. After 6 h incubation, five visual fields were randomly chosen from each well and photographed by microscope (CKX53, OLYMPUS, Japan). The tube forming results were analyzed by ImageJ.

Transwell permeability assay. An equal number of MLFs seeded in 6 cm dishes were cultivated with MCM supplemented with 10% (v/v) FBS, treated with or without peptide drugs (TP5, sFD17, FR17 at the concentration of 100 μM) for 48 h. Cells cultivated with fresh complete medium was set up as control. The pre-treated MLFs were digested and seeded at the lower well of a 24-well transwell plate at 2.5×10^5 cells per well. Each group was triplicate. Then, 7,000 Mouse endothelial bEnd3 cells were seeded on a 0.4 μm Transwell insert (Cat. 3413, Corning Costar, USA) above the top of the well until grown to confluence. Rhodamine B-dextran (70 kDa,

Cat. R9379, Sigma-Aldrich, USA) was added to the upper insert on the endothelial cell layer. After 1 h incubation, the translocation of Rhodamine B-dextran from the insert to the lower well passing through the endothelial cell layer was measured by a microplate reader (SPARK, TECAN, Switzerland) at an excitation/emission wavelength of 540 / 625 nm. The relative permeability of the cell layer was normalized by diving the fluorescence signals of the treatment groups by the control group.

Integrality of the endothelial cell monolayer. Mouse endothelial bEnd3 cells grown in 35-mm confocal dishes to 100% confluence were treated with conditional FCM, which was obtained from MLFs stimulated by MCM with or without the treatment of different peptides (TP5, sFD17, FR17 at the concentration of 100 μM) as illustrated above. After incubated with conditional FCM for 24 h, the single endothelial cell layer was gently washed with PBS and fixed with 4% paraformaldehyde for 15min, permeabilized with 0.2% Triton X-100 for 15min and blocked with 2% bovine serum albumin (BSA) for another 15 min. Cells were incubated with anti-VE-cadherin antibody (1:1000, Cat. Ab205336, Abcam, UK) containing 0.2% BSA and 0.1% Triton X-100 in PBS at 4 °C overnight. Cells were washed with PBS for three times and incubated for 1 h with AF647 labeled goat anti-rabbit IgG (H+L) (1:100, Cat. 33113ES60, Yeasen, China). The nuclei were labeled by DAPI solution (ready-to-use) (Solarbio, China). Images were taken by confocal microscope (Leica, German).

Mice and animal models. C57BL/6 mice (male, 5-week-old) purchased from Slaccas (Shanghai,

China) were adaptive fed for more than one week for subsequent experiments. The animals were maintained under standard laboratory housing conditions where foods and water can be reached freely. All the animal experiments were conducted following the guidelines which have been approved by the Ethics Committee of Zhejiang University.

For MCM-induced lung metastasis model, MCM (300 μL per mice) was intraperitoneally injected to the mice for 10 consecutive days from Day 1 to 10. On Day 7, a tail vein injection of B16F10 or Luc-B16F10 cells (1×10^5 per mice) was given to the mice. Lung metastasis was monitored twice a week by bioluminescence imaging (IVIS® Spectrum In Vivo Imaging System, PerkinElmer, USA) if viable. For bioluminescence imaging, mice were intraperitoneally injected with D-luciferin potassium salt (150 mg/kg, Gold Biotechnology, USA). The bioluminescence of pulmonary metastases was detected 10 min later.

For post-surgery metastasis model, 1×10^6 B16F10 cells were subcutaneously inoculated in the back of the C57BL/6 mice (male) aged 6 weeks above the right hindlimb on Day 1. On Day 12, tumor resection surgery was conducted on mice to remove the entire tumor tissues as well as the skin cover the tumor under anesthesia. On the next day, 1×10^5 luciferase-expressing B16F10 cells were injected into mice through tail vein. The tumor recurrence and lung metastasis were monitored twice a week. The tumor volume and body weight were recorded twice a week. Tumor volume was calculated as ($width^2 \times length$) / 2.

Pre-metastatic niche study. MCM (300 μL per mice) was intraperitoneally injected to the mice for 10 consecutive days. On Day 7, a tail vein injection of B16F10 or Luc-B16F10 cells (1×10^5

per mice) was given to the mice. On Day 3, 6, 10, 13, mice were euthanized for cardiac perfusion and the lung tissues were collected for further analysis.

For Western-blot analysis, total proteins from the lung tissues were extracted using Tissue Protein Extraction Reagent (T-PER™, Cat. 78510, Thermo Pierce, Thermo Scientific, USA) and quantified with a Bradford Protein Assay Kit (Cat. P0010, Beyotime, Beijing, China). Samples (60 μg) were separated on 10% or 8% SDS-PAGE gels, then transferred to PVDF nitrocellulose membrane (Cat. IPVH00010, Merck Millipore). Membranes were incubated with the appropriate primary antibodies in 3% BSA, including Fibronectin (1:500, Cat. ab2413, Abcam, UK), MMP9 (1:1000, Cat. ab38898, Abcam, UK), VEGFa (1:500, Cat. ab119, Abcam, UK), TGF-β1 (1:1000, Cat. ab179695, Abcam, UK), iNOS (1:1000, Cat. ab204017, Abcam, UK), Arginase 1 (1:1000, Cat. ab124917, Abcam, UK). Antibody against GAPDH (1:10000, Cat. ab181602, Abcam) was used as control. After incubation with appropriate secondary antibody Goat anti-Mouse IgG (H+L) (1:5000, Cat. 31160, Thermo Pierce) or Goat anti-Rabbit IgG (H+L) (1:5000, Cat. 31210, Thermo Pierce), the intensity of the immunoreactive proteins was stabilized by SuperSignal® West Dura Extended Duration Substrate (Cat. 34075, Thermo Pierce) and visualized on X-ray film.

For ELISA analysis, the lung tissues were ground and centrifuged to gain supernatant to measure the MMP2 (Cat. OM457413, Omnimabs, USA) and ROS (Cat. OM641674, Omnimabs, USA) level.

For immunofluorescence staining, the left lung was fixed with 4% paraformaldehyde and 30% sucrose solution overnight, and embedded into paraffin and sliced into sections. The paraffin

lung sections were deparaffinized and rehydrated, then stained with primary antibodies: αSMA (1:500, Cat. Ab7817, Abcam, UK), or CD34 (1:500, Cat. Ab81289, Abcam, UK). Secondary antibody Cy3 conjugated goat anti-rabbit IgG (1:500, Cat. 111-165-003, Jackson, USA) was utilized in 1:500 dilution and stained with DAPI before observation.

For flow cytometry analysis, lung tissues harvested from mice were mechanically minced into 1-2 mm pieces using scissors and then dissociated into single cell suspension at 37 °C on a shaker for 30 min by enzymes. The digesting solution contains 2 mg/mL collagenase I (Cat. BS163, BioSharp, Germany), 2 mg/mL collagenase II (Cat. BS164, BioSharp, Germany) and DNase I (Cat. KGF008, KeyGEN BioTech., China). Digestion was stopped by adding 2 volumes PBS and filtered through a 70 μM cell strainer (Cat. CSS013070, Jet BIOFIL®, China). The cell suspension was centrifuged at 400 g for 5 min to discard the supernatant. Cell precipitations were then resuspended in 5 mL RBC lysis buffer (Cat. R1010, Solarbio, China) and centrifuged again to discard the supernatant. The single-cell-suspensions washed with PBS and resuspended were incubated with FITC-antimouse-CD45 (Cat. 553079, BD, USA), PE-antimouse-NK1.1 (Cat. 108708, Biolegend, USA), PE-antimouse-CD3 (Cat. 100205, Biolegend, USA), PE-antimouse-TER119 (Cat. 116207, Biolegend, USA), PE-antimouse-CD19 (Cat. 152407, Biolegend, USA), APC-antimouse-CD11b (Cat. 101211, Biolegend, USA), BV605-antimouse-MHC II (Cat. 107639, Biolegend, USA), BB700-CD11c (Cat. 566505, BD, USA), BV421-antimouse-Ly6c (Cat. 562727, BD, USA) and PE/CF594-antimouse-Ly6g (Cat. 562700, BD, USA), BV711-antimouse-F4/80 (Cat. 123147, Biolegend, USA), PE/Cy7-antimouse-CD103 (Cat. 121426, Biolegend, USA) antibodies in 100 μL 1% BSA

containing 50 μL BD Brilliant Stain Buffer for 30 min at 4 °C in dark. After centrifuged and washed with PBS, cell pellets were fixed and membrane were perforated with Fix/Perm Buffer (Cat. 562574, BD, USA). The cell pellets were then stained with BV650-antimouse-CD206 (Cat. 141723, Biolegend, USA) for 40 min in the dark at room temperature. After centrifuged and washed with PBS, the stained cell pellets were analyzed by BD Fortessa flow cytometry. The data were analyzed using FlowJo software.

To investigate the impact of PMN formation induced by MCM injection, metastasis development and mice survival were monitored on MCM-induced PMN model and on the mice that didn't receive MCM injection but were inoculated directly with Luc-B16F10 cells (1×10^5 per mice) on Day 7. Lung metastasis was monitored twice a week by bioluminescence imaging (IVIS Spectrum, USA).

Influence of peptide interference on mice PMN

For mice PMN model, MCM (300 μL per mice) was intraperitoneally injected to the mice for 10 consecutive days. On Day 7, a tail vein injection of B16F10 or Luc-B16F10 cells (1×10^5 per mice) was given to the mice. Mice were randomly divided into 4 groups, namely control, TP5, sFD17 and FR17. Peptides, including TP5, sFD17 and FR17, were administrated separately to the mice subcutaneously from Day 3 at 40 μM/kg/day. On Day 10, mice were euthanized for cardiac perfusion and the lung tissues were collected for further analysis.

The lung tissues harvested from different groups were fixed, embedded into paraffin and sliced

into sections. To visualize the activation of lung fibroblasts and angiogenesis in pulmonary PMN, the paraffin lung sections after deparaffinization and rehydration, were stained with primary antibodies: αSMA (1:500, Cat. ab7817, Abcam, UK), or CD34 (1:500, Cat. ab81289, Abcam, UK). Secondary antibody Cy3 conjugated goat anti-rabbit IgG (Cat. 111-165-003, Jackson, USA) was utilized in 1:500 dilution and stained with DAPI before observation. To visualize the extracellular matrix environment alteration in pulmonary PMN, the lung sections were stained with appropriate primary antibodies: MMP2 (1:200, Cat. 10373-2-ap, PTG, USA), or MMP9 (1:1000, Cat. ab228402, Abcam, UK), Secondary antibody Cy3 conjugated goat anti-rabbit IgG (1:500, Cat. 111-165-003, Jackson, USA) and DAPI. To visualize the collagen deposition in pulmonary PMN, Masson's trichrome staining of the lung sections were imaged and analyzed by ImageJ to calculate the collagen volume fraction (CVF) by dividing the blue collagen area by total tissue area. And the Sirius Red Staining was also carried out and the sections were visualized under the polarizing microscope (Nikon Eclipse Ci). To investigate the recruitment of MDSC in PMN, serial sections of lung tissues were stained with periostin (1:200, Cat. 19899-1-AP, PTG, USA), or co-stained with LOX (1:200, Cat. ab174316, Abcam, UK) and Fibronectin (1:200, Cat. ab92572, Abcam, UK) antibody, or CD11b (1:2000, Cat. ab133357, Abcam, UK) and Gr-1 (1:200, Cat. ab25377, Abcam, UK) antibody separately. Secondary antibody Cy3 conjugated goat anti-rabbit IgG (1:500, Cat. 111-165-003, Jackson, USA), goat anti-rabbit IgG conjugated to HRP (1:2000, Cat. ab6721, Abcam, UK) and fluorescent TSA-488 (1:200, Wuhan Pinuofei, China) were applied according to Tyramide Signal Amplification technology. The stained sections were observed and imaged under the confocal microscope. Images were analyzed by ImageJ if necessary.

To investigate the alteration of protein expression level in PMN, Western-blot or ELISA experiments were carried out. For Western-blot assay, protein samples were extracted separately from three independent mice from each group. Total proteins from the lung tissues were extracted using Tissue Protein Extraction Reagent (T-PERTM, Cat. 78510, Thermo Pierce, Thermo Scientific, USA) and quantified with a Bradford Protein Assay Kit (Cat. P0010, Beyotime, Beijing, China). Samples (60 μg) were separated on 10% or 8% SDS-PAGE gels, then transferred to PVDF nitrocellulose membrane (Cat. IPVH00010, Merck Millipore). Membranes were incubated with the appropriate primary antibodies in 3% BSA, including Fibronectin (1:500, Cat. ab2413, Abcam, UK), Versican (1:1000, Cat. ab270445, Abcam, UK), VEGFa (1:500, Cat. ab119, Abcam, UK), ANG2 (1:500, Cat. ab155106, Abcam, UK), MMP9 (1:1000, Cat. ab38898, Abcam, UK), MMP2 (1:500, Cat. ab97779, Abcam, UK), TGF-β1 (1:1000, Cat. ab179695, Abcam, UK). Antibody against GAPDH (1:10000, Cat. ab181602, Abcam) was used as control. After incubation with secondary antibody Goat anti-Mouse IgG (H+L) (1:5000, Cat. 31160, Thermo Pierce) or Goat anti-Rabbit IgG (H+L) (1:5000, Cat. 31210, Thermo Pierce), the intensity of the immunoreactive proteins was stabilized by SuperSignal® West Dura Extended Duration Substrate (Cat. 34075, Thermo Pierce) and visualized on X-ray film. For ELISA assay, lung tissues were ground and centrifuged to gain supernatant to measure the IL-6 (Cat. EK0411, Boster, China) level.

***In vivo* vascular permeability assay.** MCM (300 μL per mice) was intraperitoneally injected to the mice for 7 consecutive days. And the mice were randomly divided into 4 groups, namely

control, TP5, sFD17 and FR17. Peptides, including TP5, sFD17 and FR17, were administrated separately to the mice subcutaneously from Day 3 at 40 μM/kg/day. On day 7, 100 mg/kg Rhodamine B-dextran (70 kDa, Cat. R9379, Sigma-Aldrich, USA) was intravenously injected to the mice. After 3 h, mice were injected with FITC-lectin (Cat. L0770, Sigma-Aldrich, USA) at 10 mg/kg through the tail-vein. Ten minutes later, each mouse was anesthetized and transcardiac perfused with 20 mL saline to remove the excess dye and followed by 5 mL of 4% formaldehyde. The lung tissues were formaldehyde-fixed and cryo-sectioned. Slices were observed and imaged by fluorescence microscopy for vascular leakage. There were 3 mice in each group and 5 visual fields were randomly chosen for each section. The relative vascular permeability was analyzed by dividing the dye leakage of each group by healthy control.

Recruitment of MDSC to PMN. On Day 10 of PMN mice model, lung tissues were harvested from different treatment groups and mechanically minced and digested to obtain the single-cell-suspensions as described above. The single-cell-suspensions washed with PBS and resuspended were incubated with APC-antimouse-CD11b (Cat. 101211, Biolegend, USA) and PE/Cy7-antimouse-Ly6g (Cat. 127617, Biolegend, USA) antibodies in 100 μL 1% BSA for 30 min at 4 °C in dark. After centrifuged and washed with PBS, cell pellets were analyzed by BD Fortessa flow cytometry. The data were analyzed using FlowJo software.

mRNA sequencing of $CD11b^{+}Ly6g^{+}$ MDSC recruited to PMN. On Day 10 of PMN mice model, lung tissues were harvested from different treatment groups and digested into single cells

as introduced as above. The single-cell-suspensions after washing with PBS and re-suspension were incubated with APC-antimouse-CD11b (Cat. 101211, Biolegend, USA) and PE/Cy7-antimouse-Ly6g(Cat. 127617, Biolegend, USA) antibodies in 100 μL 1% BSA for 30 min at 4 °C in the dark. After centrifuged and washed with PBS, $CD11b^{+}Ly6g^{+}$ MDSCs were sorted from the PMN lungs of 10-12 individual mice from each group per sample by FACS (Beckman moflo Astrios EQ). Total RNA was extracted by TRIzol for cDNA preamplification using the NEBNext® Ultra™ Directional RNA Library Prep Kit for Illumina®, then analyzed using Qubit2.0 Fluorometer, Agilent 2100 bioanalyzer and qRT-PCR. Significantly enriched gene sets were defined as P values < 0.05 comparing to the control group.

Inhibition of tumor metastasis on MCM-induced PMN lung metastasis model. The PMN models were established as introduced above, mice were randomly divided into 4 groups (n = 7), namely control, TP5, sFD17 and FR17. From day 3 to 21, mice from different groups were subcutaneously administrated with saline, TP5 (40 μM/kg per day), sFD17 (40 μM/kg per day) and FR17 (40 μM/kg per day) separately. Body weight was recorded every 3 days. On day 20, blood was collected from the submarginal ocular venous plexus under anesthesia for blood tests including complete blood count, alanine aminotransferase (ALT), aspartate aminotransferase (AST), blood urea nitrogen (BUN) and serum creatinine (CREA). On day 28, mice were euthanized and major organs, such as heart, liver, spleen, lung, kidney and thymus were collected after cardiac perfusion. Lung tumor nodules were then counted under the stereo microscope. The major organs were fixed, embedded into paraffin for Hematoxylin & Eosin staining. The thymus

coefficient was calculated as the thymus weight divided by the body weight and the spleen coefficient was calculated as the spleen weight divided by the body weight.

Inhibition of tumor metastasis post-surgery. The post-surgery metastasis model was established as illustrated above. Mice were randomly divided into 3 groups, namely control, anti-PD1 and FR17. For FR17 treatment, peptide was subcutaneously administrated to the mice from Day 7 to Day 25 at the dose of 40 μM/kg per day. For anti-PD1 treatment, 100 mg anti-PD1 (Cat. BE0146, Bio X Cell, USA) was given by *i.p.* injection twice per week starting from day 3 post tumor resection and given two times per week from Day 15 to Day 25 for a total of 4 times. Lung metastasis was monitored twice a week by bioluminescence imaging (IVIS Spectrum, USA) until death. The recurrence of the excised subcutaneous tumor was closely monitored and tumor volume was measured and calculated following the ellipsoid volume formula: $(\text{width}^2 \times \text{length}) / 2$.

Statistics

Statistical analysis was performed using GraphPad Prism 8.0.1 (GraphPad Software, CA, USA). Data were presented as means ± SD. Statistical evaluation of differences between experimental groups was performed by one-way ANOVA followed by Tukey's multiple comparisons test. Statistical significance was considered at least at $p < 0.05$.

[1] Abraham, M. J. et al. GROMACS: High performance molecular simulations through multi-level parallelism from laptops to supercomputers. *SoftwareX*, **1**, 19-25 (2015).

[2] Humphrey, W., Dalke A. & Schulten, K. VMD: visual molecular dynamics. *J. molecular graphics*, **14**, 33-38 (1996).

Supplementary Files

This is a list of supplementary files associated with this preprint. Click to download.

- SIV9.pdf
- SIV9withoutauthorsinformation.pdf
- SIV9withoutauthorsinformation.pdf
- nrreportingsummary20210809T100118.224.pdf